Numerical Simulation in Electrical Cardiometry

Alexandru M. Morega[1,2], *Senior Member, IEEE*, Alin A. Dobre[1], *Student Member, IEEE*, Mihaela Morega[1], *Member, IEEE*
[1]University POLITEHNICA of Bucharest, Faculty of Electrical Engineering, Bucharest, ROMANIA
[2]"Gheorghe Mihoc – Caius Iacob" Institute of Statistical Mathematics and Applied Mathematics, Romanian Academy
amm@iem.pub.ro, alin_dobre@yahoo.com, mihaela@iem.pub.ro

***Abstract*- This study is concerned with the direct problem of Electro Cardiometry (ECM) technique, and the associated thoracic electrical bioimpedance (TEB). We present a mathematical model for the hemodynamic of the aorta, the change in the electrical conductivity of the blood, and the electrical field problem equivalent to the ECM procedure.**

Having in view that anatomy plays a key role in investigating the ECM-TEB problem we used a 3D computational domain produced by medical image based reconstruction techniques.

The mathematical model is solved by numerical simulation in the finite element method (FEM) technique. Analytic formulae for the electrical conductivity of the blood are available, however, when investigating the hemodynamic of the aorta flow considering an anatomically realistic computational domain, these results are difficult (if possible) to use as such. To circumvent this difficulty we defined an equivalent conductivity based on analytic results, by averaging techniques that outline the sensitivity of TEB to the aorta blood flow dynamics.

The work reported here addresses the direct problem of ECM-TEB, aiming at assessing the sensitivity of TEB to the flow parameters. Its solution opens the path to the inverse EMC-TEB problem, with the objective of deciphering the flow dynamics out of EMC-TEB experimental data.

I. INTRODUCTION

Localization and genesis of vascular disease in regions of complex flow in the coronary, carotid, abdominal, and femoral arteries are due to hemodynamic factors, and both invasive and noninvasive monitoring techniques aimed to investigate the blood flow and its relation to the cardiac activity are of a particular interest. In this area of concern, the pulsatile flow in the abdominal aorta may be related to the *Impedance Cardiography* (ICG).

ICG senses changes in the electrical impedance across the thoracic region over the cardiac cycle: lower impedance indicates greater intra-thoracic fluid volume and blood flow [1]. By synchronizing fluid volume changes with the heartbeat, the change in the *Thoracic Electrical Bioimpedance* (TEB) can be used to calculate the *Stroke Volume* (SV), the *Cardiac Output* (CO), and the *Systemic Vascular Resistance* (SVR) [1-5]. Technically, ICG measures TEB, which echoes the volumetric changes in the ascending aorta following aortic valve opening.

Recently, a noninvasive TEB method, called *Electrical Velocimetry*, leading to a new method called *Electrical CardioMetry*[1], (ECM) was reported [2,3].

ECM senses the changes in the conductivity of the blood in the aorta during the cardiac cycle, and relates the steep increase in TEB to the beat-to-beat change in orientation of red blood cells (RBCs).

ECM utilizes an array of 4 surface ECG electrodes attached to the left side of the neck and the lower thorax. An electrical alternating current (AC) of constant amplitude is applied to the thorax through the outer pair of electrodes and in particular – because blood is the most conducting medium in the thorax – the ascending and descending aorta. The resulting voltage and eventually a surface ECG are obtained via the inner pair of electrodes. The ratio of applied current and measured voltage is recorded over time [2].

The measured TEB over time can be expressed as the superposition of three components

$$Z(t) = Z_0 + \Delta Z_R + \Delta Z_C \,, \tag{1}$$

where Z_0 is the quasi-static impedance (*base impedance*), mostly contributed by thoracic fluids including the thoracic blood volume; ΔZ_R are the changes of impedance due to respiration, and ΔZ_C are the changes of impedance due to the cardiac cycle. ΔZ_R is considered an artifact to the estimation of stroke volume and, thus, suppressed [2]. The dynamics of ΔZ_C resembles the arterial blood pressure waveform.

Several models for estimating SV based on TEB are available [5]. The shape of the inverted TEB waveform, is akin the conductivity waveform, and since TEB also shows resemblance with the arterial pressure waveform, it has become common use to display the inverted $Z(t)$, and read it as a change-of-conductivity waveform [2].

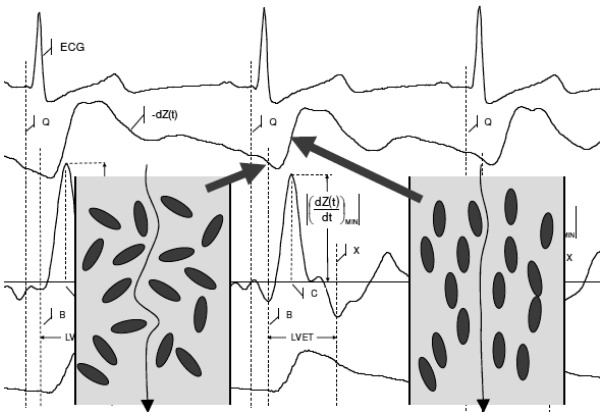

Fig. 1. Timely course of parallel recordings of ECG, impedance waveforms and pulse plethysmogram, and the red blood cells orientation in the aorta prior and shortly after aortic valve opening – image from [2].

The change in the electrical conductivity of blood is explained as follows. Prior to opening of aortic valve, the RBCs are randomly oriented since there is no net blood flow in the aorta (Fig. 1). An applied electrical current sweeps the

[1] Electrical Cardiometry is a method trademarked by Cardiotronic, Inc. www.cardiotronic.net. ECM monitors have shown promise in postoperative cardiac surgical patients [3].

red blood cells (RBCs) for passing through the aorta, which results in a higher voltage drop (a longer path), hence lower electrical conductivity.

The electrical conductivity of blood is subject of intense research, and quantitative theories that explain the blood conductivity dependency on the flow in Poiseuille flows are available (*e.g.*, [6]). For low-frequency (1 MHz) alternating currents the conductivity of RBCs is much lower than the conductivity of plasma, and the disintegration of rouleaux (chains of RBCs) at very low flow velocities as well as the orientation and deformation of RBCs results in a change of the current pathway in the plasma, hence in a change of the conductivity. Therefore, both orientation and deformation of RBCs contribute to the change in the conductivity of blood.

In recent years computational techniques have been used increasingly by researchers seeking to understand vascular hemodynamic. These methods can augment the data provided by in vitro and in vivo methods by enabling a complete characterization of hemodynamic conditions under precisely controlled conditions. This study is concerned with developing a mathematical model for the ECM-TEB procedure. The model accounts for the unsteady pulsating aorta flow, the change in the electrical conductivity of the blood, and the electrical field associated to the ECM-TEB measurement. The model is solved by numerical simulation, in the finite element technique (FEM). The computational domain is obtained by reconstruction techniques out of medical scans.

II. The Electrical Conductivity of the Blood

In this study we use the results reported by [6], [7] and [8] to define an equivalent conductivity for the blood, which is assumed as a flowing dilute suspension of ellipsoidal particles (the RBCs) in plasma. Each ellipsoid has two long axes (b) and one short axis (a), where $a < b$. Maxwell–Fricke equation may be used to determine the conductivity of a suspension of RBCs in a low-frequency alternating electrical field.

These studies demonstrate that during accelerating flow (through a round, straight tube of radius r_0), the impedance change (or orientation response) follows without delay any change in flow. Conversely, during deceleration of flow, an exponential decay in orientation occurs with a time constant ranging in the order of 1 to 100 s. An approximate expression of the orientation rate is [7]

$$f(r) = \frac{n}{n_0}\frac{\tau_0^{-1}(r)}{\tau_d^{-1}(r)+\tau_0^{-1}(r)}, \qquad (1)$$

where r is the radius ($r <= r_0$), n is the number of RBCs with stable orientation per unit volume (assumed to be oriented parallel to the flow), n_0 is the total number of RBCs per unit volume, τ_0 is the time constant for cells changing from random to aligned orientation and τ_d is the time constant for cells randomization. The time constant for cell orientation (τ_0) is proportional to the inverse of the shear rate and the time constant for cell disorientation (τ_d) is proportional to the inverse of the square root of the shear rate.

The deformation of RBCs in shear flow is related to the resulting shear stress in the fluid. The shear rate, τ_w – a local quantity – is approximated here, in the order of magnitude sense, by the average friction factor [10]. In fully developed Hagen-Poiseuille flow through a round tube

$$\tau_w = \mu\left(-\frac{du}{dr}\right)\Big|_{r=r_0} = 4\mu\frac{U}{r_0}, \qquad (2)$$

where U is the average velocity, μ is the dynamic viscosity.

In this study we use realistic, medical image based computational domain to numerically simulate the aorta blood flow rather then round tubes. To circumvent the difficulty of applying these analytic findings we define the *equivalent* round tube for the aorta as follows: (1) the radius r_0 is computed based on the average inlet to outlet cross-sections areas; (2) the tube length is the ratio aorta volume / average cross-section area; (3) the velocity U is the computed out of the mass flow rate.

Fig. 2 shows the equivalent shear rate τ_w produced by numerical simulation results. On the other hand, depending on τ_w, [6] predicts analytic formulae for the local conductivity of the blood. In this case ($\tau_w > 0.1$ N·m^{-2})

$$\frac{\sigma_b}{\sigma_{pl}} = \frac{1-H}{1+(C-1)H}, \qquad (3)$$

is recommended. In (3) σ_b and σ_{pl} are the conductivities (S·m^{-1}) of blood and plasma, respectively, H is the hematocrit expressed as a fraction, C is a factor that depends on the geometry of the RBC.

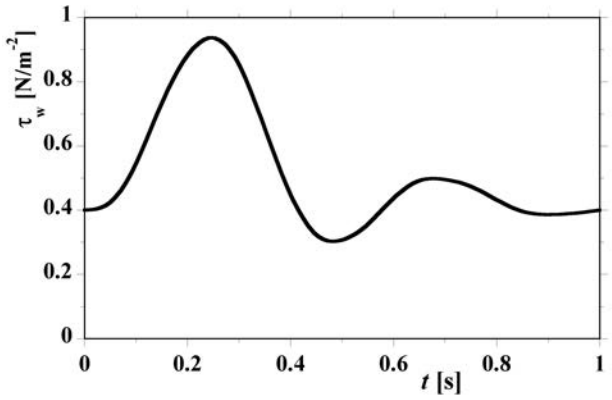

Fig. 2. The equivalent shear rate, τ_w.

The factor C (a function of r in the round tube theory [7]) is evaluated for $r = r_0$

$$C(r_0) = f(r_0)\cdot C_b + \left[1-f(r_0)\right]\cdot C_r, \qquad (4)$$

$C_r = (C_a + 2C_b)/3$, $C_a = 1/M$, $C_b = C(r_0) = 2/(2-M)$, $M(a<b) = \cos(\varphi)\cdot\left[\varphi - \sin(2\varphi)\right]/\sin^3(\varphi)$, $\cos(\varphi) = a/b$. The calculations where performed for a/b = 0.38 (an average value [7]), which yields $M \cong a/b$.

III. The Computation Domain – An Image Based Reconstruction Approach

Realistic computational domains are crucial for generating physically meaningful results to medical physics problems. The complex morphology of the anatomical organs and tissues play a key role in numerical modeling and simulation procedures, when used as computation domains. CT/MRI good quality images provide data on accurate geometry and anatomical structure, while 3D high-resolution reconstruction techniques lead to realistic computational domains.

We used here a publicly available medical image dataset of the whole body [11], comprised of approx. 500 MRI images. Successive numerical procedures were applied to the DICOM original images using specialized software [12,13]. The anatomical regions of interest identified for the ECM problem (*i.e.* brain, bones, spinal cord, lungs, myocardium, aorta, liver and thorax) were subjected to a numerical segmentation process and the shapes of the mentioned organs were properly designated; filtering and smoothing procedures were further applied in order to eliminate noise and unwanted regions. Fig. 3 shows examples of processed slices. For the final purpose of the model, only the upper half of the body was retained.

Fig. 3. The segmented masks of the regions of interest.

After the segmented masks were post processed and given the final shape by applying different combinations of the optimized filters, a set of subtraction, inversion and intersection Boolean operations [13] was necessary. The final, cut-out-of-the-body 3D solid models (Fig. 4,b) are ready to be meshed as a computational domain.

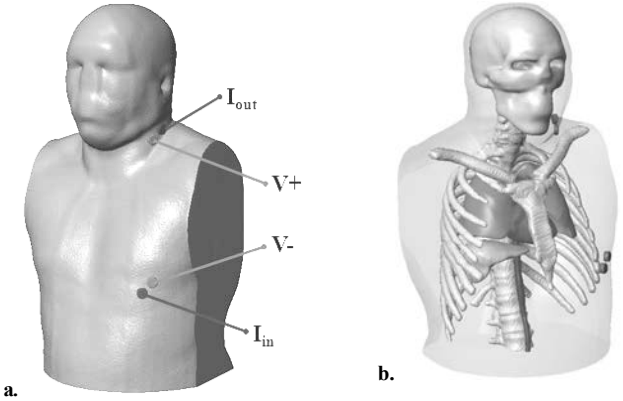

Fig. 4. The final shape of the segmented masks: (a) electrodes for ECM numerical simulations; (b) the translucent thorax with internal organs.

Our multipart 3D model was discretized using the voxel and volumetric marching cube (VoMaC) grid-based meshing methods [13], generating a multipart FEM discretized computation domain (Fig. 5). The voxel approach combines the geometry detection and the mesh generation in one step: after the voxels are classified during a certain segmentation process, they are directly exported as hex elements.

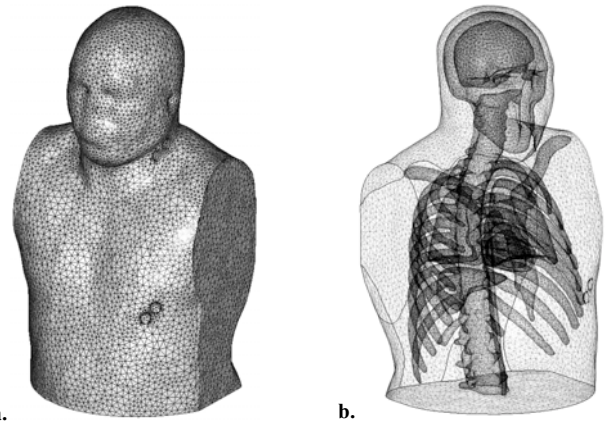

Fig. 5. The multipart computational domain mesh made of approximately 565,000 tetrahedral elements: external surface (a) and interior parts view (b).

IV. Mathematical Model for the Direct Electrocardiometry Problem

The solution to the ECM problem follows two steps. First, the blood flow in the abdominal aorta is solved for. The heart, although included in the computational domain, is not part of the hemodynamic problem. The aortic flow is confined to a volume delimited by two cross-sectional interfaces (Fig. 6). This stage provides for the (dynamic) electrical conductivity of the blood (Section II). Next, the electrical field problem is solved. In this study we use the equivalent electrokinetic model that provides the effective values for the quantities utilized in computing the TBE and its derivates. The validity of this approach is justified by the fact that for frequencies below several hundred kilohertz, the impedance of blood can be considered purely resistive, because the charging time of the RBC membranes is small enough to charge and discharge the membrane completely during a single cycle [6].

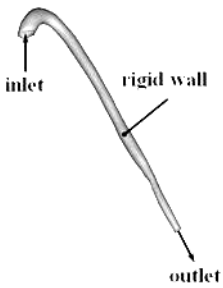

Fig. 6. The boundary conditions that close the hemodynamic problem.

The electrical impedance (TEB), Z [Ω], is computed by $Z = U/I$, where U is the measured electrical voltage [V] and I is

the external, excitation current (here I_{in} = 400 μA, injected in the sidewise abdominal region, see Fig. 4,a). TEB and its time derivative are usually correlated with the electrocardiography (ECG) waveforms to obtain accurate and meaningful results. More details regarding the ICG and ECM noninvasive techniques for monitoring hemodynamic properties of blood flow, as well as a set of 3D models useful in the simulation and analysis of these procedures can be found in [14,15].

A. The Hemodynamic Model

Although RBCs have a key role in the ECM, we assumed the blood as a Newtonian fluid, with constant properties. This assumption is consistent with the hemodynamic of large arteries (*e.g.*, the aorta). Its flow is pulsatile, laminar, and incompressible [15,16], described by

momentum balance (*Navier-Stokes*)

$$\rho\left[\frac{\partial \mathbf{u}}{\partial t}+(\mathbf{u}\cdot\nabla)\mathbf{u}\right]=\nabla\left[-p\mathbf{I}+\eta\left(\nabla\mathbf{u}+(\nabla\mathbf{u})^{T}\right)\right], \quad (5)$$

the mass conservation law

$$\nabla\cdot\mathbf{u}=0, \quad (6)$$

where **u** [m/s] is the velocity field, p [Pa] is the pressure, ρ [kg/m^3] is the mass density [1050 kg/m^3], and **I** is the unity matrix. The dynamic viscosity of the blood, η [Pa·s] is [6]

$$\eta=\eta_{pl}\left(1+2.5H+7.37\times10^{-2}H\right), \quad (7)$$

where η_{pl} = 1.35×10^{-3} Pa·s is the viscosity of plasma.

The boundary conditions that close the model are set as follows (Fig. 6). For the inlet, we set the uniform, periodic profile derived from the Womersley theory [17], Fig. 7.

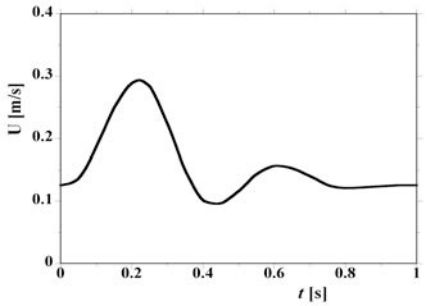

Fig. 7. Inlet boundary conditions for the hemodynamic problem [17].

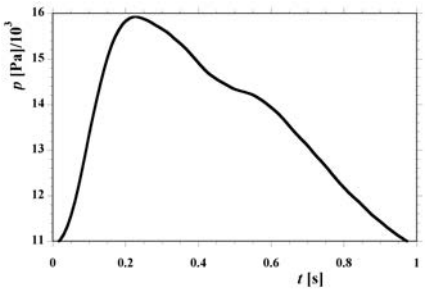

Fig. 8. Outlet boundary conditions for the hemodynamic problem.

On the other hand, for the outlet, the uniform, periodic pressure profile shown in Fig. 8 is set. The blood flow – structural interaction is neglected due to the low deformations that occur in this type of large arteries [15,16].

B. The Electrical Field Model

The EMC equivalent electrokinetic model is described by

$$\Delta V=0, \quad (8)$$

where V is electrokinetic potential. The surface of the thorax is assumed electrically insulated (**n**·**J** = 0; **J** is the electrical current density and **n** is the outer normal). The pair of "voltage" electrodes has floating potential conditions. The "current" electrodes have prescribed inward current and ground, respectively (Fig. 9).

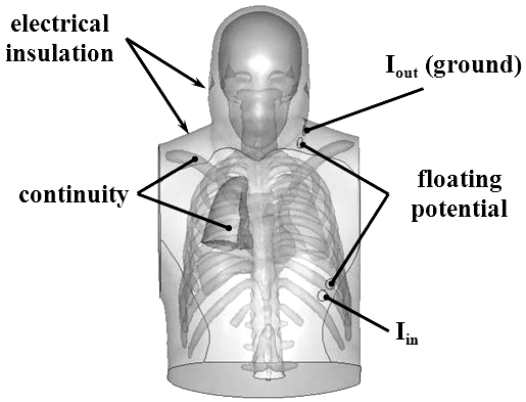

Fig. 9. The boundary conditions set for the electrical field problem.

The volume conductor of the thorax was carefully cropped, considering that electrical insulation boundary conditions are set there.

V. Numerical Simulation Results

The mathematical model was solved numerically by Galerkin finite element method (FEM), as implemented by Comsol Multiphysics [19]. To comply with the available hardware and software limits, we solved first the hemodynamic problem. Several tests were performed to ensure the numerical accuracy (*e.g.*, three-four cardiac cycles are sufficient to reach periodic flow conditions). The electrical field problem was then solved, using the flow results needed to compute the conductivity of blood that were saved throughout the simulation of the last period. Lagrange linear (for the electrical field) and P1-P2 (for the flow) elements were used to FEM approximate the solution [19].

Fig. 10 displays a composite image of the aorta flow (velocity arrows), electrical current density flux tubes, and the electric potential (gray map). The current density flux finds the aorta as a higher conductivity, channeling path. The time variation of the blood conductivity "tunes" this current path between some min-max limits. This process is echoed by the TEB. In this study, the direct TEB problem is of concern (evaluate TEB sensitivity to known flow dynamics), and the results may be used to build a solution to the inverse TEB problem: given the TEB (*e.g.*, by ECM), find the flow dynamics parameters.

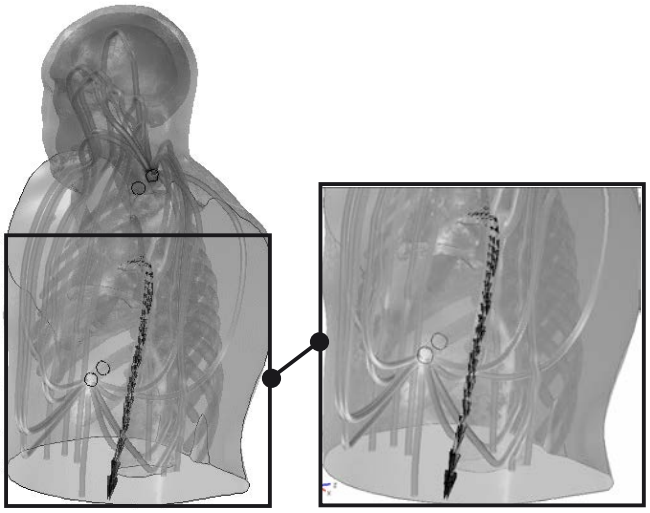

Fig. 10. Gray maps of electric potential, and stream (flux) tubes of electrical current density.

Fig. 11,a shows TEB experimental data [20], and Fig. 11,b displays the TEB waveforms obtained out of our numerical simulations. In fact, Fig. 11 shows the traditional inverse depiction of the TEB [21]. Considering the simplifying assumptions – *e.g.*, the electrical activity of the heart, the hemodynamic of the heart – the numerical simulation is in good agreement with the experiment in that the morphology of TEB and its derivative are satisfactorily well rendered. The numerical results confirm that the underlying phenomenon evidenced by ECM (TEB dynamics) is actually echoing the blood flow in the aorta. Thus, the particular hemodynamic flow events are noticeable: **B**, the start of ejection of blood by the left ventricle; **C**, the major upward deflection occurring during systole; **X** the closure of the aortic valve; **O**, the diastolic upward deflection; LVET, the left ventricular ejection time, and dZ/dt_{max} the maximal impedance change during systole. Interesting enough, finer details, such as the A-wave[2] emergence are also satisfactorily well revealed, suggesting that the inlet flow profile, which was used, bears the upstream, cardiac flow specificity.

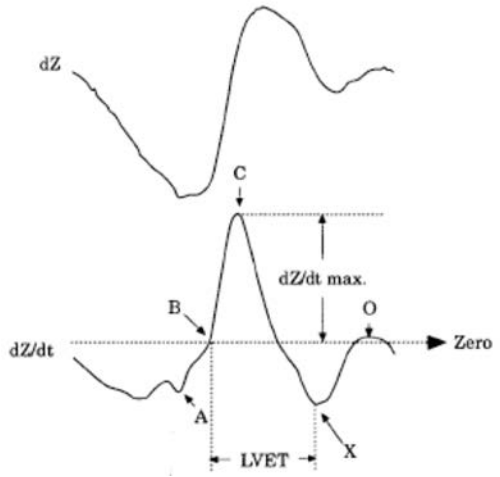

a. Experimental data [20].

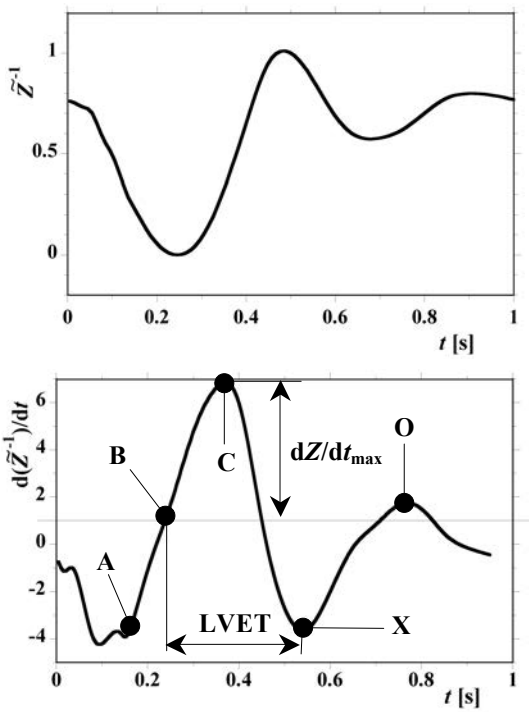

b. Numerical simulation results. $\tilde{Z}$ is the normalized (nondimensional) bioimpedance $Z(t)$.

Fig. 11. The bioimpedance and its time derivative.

VI. Conclusions

This study is concerned with the TEB as produced by the ECM procedure. Several general aspects specific to the electric velocimetry, impedance cardiography, and electrical cardiometry are presented first.

The paper presents a mathematical model for the hemodynamic of the aorta, the change in the electrical conductivity of the blood, and the electrical field problem equivalent to the ECM procedure.

It is considered that the aorta blood flow is accompanied by changes in specific electrical properties of the blood, observable by investigation procedures of electrical nature.

One major concern in numerical simulation was the computational domain. Using simplified, "geometric" computational domains may lead to great simplifications in solving the mathematical model, but the approach of the numerical results to the experiment may be questionable. Having in view that anatomy plays a key role in investigating the ECM-TEB problem we used a 3D computational domain produced by medical image based reconstruction techniques. Although we used third party software to build the computational domain, the task of conveniently yet accurately

[2] The exact contributions of the right and left atria to the A-wave, however, are not known [19]. The A-wave is linked to the contraction of the atria. Other sources conjecture that this wave has its source in the back flow of blood from the atria into the central veins. Evidence was found that the left atrium might be the main contributor to this wave, and that the left atrial ejection fraction is highly correlated to the relative height of the A-wave.

representation of anatomic entities is a nontrivial one.

The mathematical model was then solved by numerical simulation in the FEM technique. To contain the arithmetical load of a 3D model, the hemodynamic and the electric field problems are solved sequentially. The unsteady, pulsatile flow problem was solved first. The main outcome is the electrical conductivity of the blood. Analytic models that provide accurate formulae accounting for the different processes that contribute to the electrical conductivity of blood in straight, round tubes with rigid walls, the RBCs streamwise degree of orientation, the RGB mechanical interaction (stretching, compression) entrained in the plasma, viscous flow are available. However, when investigating the hemodynamic of the aorta flow considering an anatomically realistic computational domain, these results are difficult (if possible) to use as such. To circumvent this difficulty we defined an equivalent conductivity out of analytic results via averaging techniques. Consequently, several effects (*e.g.*, the uneven change in conductivity for accelerating and decelerating flow) may not be evidenced, but the sensitivity of TEB to the aorta flow dynamics is clearly distinguishable.

The ECM-TEB and its derivative found by numerical simulation compares satisfactorily well with available experimental data, and relevant flow parameters are clearly evidenced by the numerical results (Fig. 11: the start of ejection of blood by the left ventricle; the major upward deflection occurring during systole; the closure of the aortic valve; the diastolic upward deflection; the left ventricular ejection time, and dZ/dt_{max}).

The work reported here addresses the direct problem of ECM-TEB, aiming at assessing the sensitivity of TEB to the flow parameters. Its solution opens the path to the inverse EMC-TEB problem, with the objective of unveiling the flow dynamics out of EMC-TEB experimental data. This makes the object a future research.

ACKNOWLEDGMENTS

The first author acknowledges the support of the CNCSIS PCCE-55/2008 grant. The second author acknowledges the support offered by the POSDRU/88/1.5/S/61178 grant.

REFERENCES

[1] D.P. Bernstein, "Impledance cardiography: Pulsatile blood flow and the biophysical and electrodynamic basis for the stroke volume equations", J. of Electrical Bioimpedance, **1**, 1, pp. 2-17, 2010.

[2] M. Osypka, "An Introduction to Electrical Cardiometry", Electrical Cardiometry™ 12 Jan 2009, pp. 1-10, www.cardiotronic.net

[3] D.P.Bernstein, M.J. Osypka, "Apparatus and method for determining an approximation of stroke volume and cardiac output of the heart", US Patent No. 6,511,438.

[4] D.J. Funk, E.W. Moretti, T.J. Gan, "Minimally invasive cardiac output monitoring in the perioperative setting". Anesth. Analg. **108**, 3, pp. 887–97, 2009. doi:10.1213/ane.0b013e31818ffd99

[5] M.C. Ipate, A.A. Dobre, A.M. Morega, "The Stroke Volume and the Cardiac Output by the Impedance Cardiography," UPB Scientific Bulletin, ISSN 1454-2331, submitted.

[6] A. E. Hoetink, Th. J. C. Faes, K. R. Visser, and R. M. Heethaar, "On the Flow Dependency of the Electrical Conductivity of Blood", IEEE Trans.on Biomedical Eng., **51**, 7, pp. 1251-1261, July 2004.

[7] R.L. Gaw, B.H. Cornish, B.J. Thomas, "The electrical impedance of pulsatile blood flowing through rigid tubes: A theoretical investigation", IEEE Trans. on Biomed. Eng., **55**, 2, pp. 721-727, 2008.

[8] K.R. Visser, "Electric conductivity of stationary and flowing human blood at low frequencies", Clinical Instrumentation I, 1540--IEEE EMBS, 11th Annual Intl. Conference, © 770-6/89/0000-1540, 1989

[9] R. Smith, "A novel cartesian grid method for complex aerodynamic CFD applications," Proc. 5th Int. Conf. on Numerical Grid Generation in Computational Field Simulations, Mississippi State University, 2006.

[10] A. Bejan, *Heat Transfer*, J. Wiley & Sons, Inc., NY, pp. 295-298, 1993.

[11] Visible Human Project, U.S. National Library of Medicine, National Institutes of Health.

[12] ScanIP, +FE and +CAD Reference Guide, Simpleware Ltd., UK, 2010.

[13] *** Simpleware 4.2, Simpleware Ltd., UK, 2010.

[14] A.A. Dobre, M.C. Ipate, A.M. Morega, "The Impedance Cardiography for Blood Flow Properties Monitoring," Bulletin of Micro and Nanoelectrotehnologies, emerging article, ISSN 2069-1505.

[15] A.A. Dobre, A.M. Morega, M. Morega, "The Investigation of Flow – Structural Interaction in an Arterial Branching by Numerical Simulation," IFMBE Proc. of the 10th IEEE International Conference on Information Technology and Applications in Biomedicine ITAB 2010, 2-5 November, Corfu, Greece.

[16] A.M. Morega, A.A. Dobre, M. Morega, "Numerical Simulation of Magnetic Drug Targeting with Flow-Structural Interaction in an Arterial Branching Region of Interest," Proc. of the Comsol Users Conference, pp. 17-19, November, 2010, Paris, France.

[17] C.A. Taylor, T.J.R. Hughes, C.K. Zarins, "Finite Element Modeling of Three-Dimensional Pulsatile Flow in the Abdominal Aorta: Relevance to Atherosclerosis", Annals of Biomedical Eng., 26, pp. 975–987, 1998.

[18] A.A. Dobre, A.M. Morega, "Blood Flow-Vessel Interaction in a Subclavian Aneurysm," INCAS Bulletin, **3**, 4, pp. 59-65, October - December 2011, ISSN 2066-8201.

[19] Comsol Multiphysics, AB, v. 3.5a, 4.2a, 2010-2012.

[20] H.H. Woltjer, H.J. Bogaard, P.M.J.M. de Vries, "The technique of impedance cardiography", European Heart J., **18**, pp. 1396-1403, 1997.

[21] J. Vedru, "Electrical impedance methods for the measurement of stroke volume in man: state of art", Institute of General and Molecular Pathology Group of Biomedical Engineering, Veski 34, EE2400 Tartu, Estonia, Estonian Science Foundation grant No. 272.